The Characteristics of Microtremors at the Site of SMART1 Array

WIN-GEE HUANG
AND
YEONG-TEIN YEH
Institute of Earth Sciences
Academia Sinica, Taipei, Taiwan, R.O.C.

(Received 10 July 1990; revised 29 September 1990)

ABSTRACT

In this study, three microtremor observations were conducted in the SMART1 area, on July 12, 13 and 15, 1982. The data, in each observation, were recorded by a small circular array of about 460 m in diameter. The array consisted of 9 receivers spaces from 100 to 400 meters apart. The origin and characteristics of microtremors were investigated by the technique of high-resolution frequency-wavenumber (f-k) analysis. Our results show that microtremors, in the frequency range of 0.72 to 1.84 Hz, may be caused by the effects of the Pacific Ocean tide on the coast to the east of the Lanyang plain. The microtremors are composed of surface waves. Two-layer subsurface velocity structures are also estimated from the resulting dispersion curves. The top layer is about 112 m thick with an S-wave velocity of 390-500 $m\ s^{-1}$. The second layer is about 188 m thick with an S-wave velocity of 690-850 $m\ s^{-1}$.

1. INTRODUCTION

Microtremors (background seismic noise or earth noise) have been studied by many authors (Capon, 1969a; Haubrich and Macamy, 1969; Bungum and Rygg, 1971; Douze and Laster, 1979; Liaw and McEvilly, 1979; Oppenheimer and Iyer, 1980) using array data. Asten and Henstridge (1984) reviewed this literature and concluded that cultural sources, coastal effects, ocean storms and atmospheric loading are four main types of microtremor origins which can be identified within the frequency range of 0.5 to 3 Hz. The first two sources generate mainly Rayleigh waves; the third generates P waves, and the fourth generates undefined modes. This review also suggested that the microtremors are mainly composed of Rayleigh waves, if they are observed during a time

when no special conditions, such as low pressure, geothermal or wind actions, are present.

Many attempts have already been made to infer local geological conditions from microtremors. The methods include the use of predominate frequencies (Kanai and Tanaka, 1961) or power spectra (Katz, 1976) to determine shallow geological conditions. In both of these methods it is difficult to identify the source and propagation effects of microtremors. One of the problems which still remains with use of the above two methods (Horike, 1985), is the difficulty in distinguishing whether predominant frequencies are caused by surface waves or by body waves. The identification of wave types is an important problem because predominant frequencies of body waves caused by local conditions do not always agree with those of surface waves. In order to overcome this problem, we can identify wave types from horizontal phase velocities obtained by array data (Horike, 1985). If the measured phase velocities are less than the S-wave velocity of the basement rock and are dispersive, they may be identified as those of surface waves. If not, they will be those of body waves.

In this study, in the vicinity of the SMART1 array area, the data from three small arrays were recorded at different time periods to study the microtremors. The f-k analysis was used to identify the origin and characteristics of the microtremors. Shallow geological conditions beneath the SMART1 were also estimated from measured dispersion curves.

2. INSTRUMENTATION

The SMART1 array is situated near Lotung city in the south of the Lanyang plain, in northeastern Taiwan. Our microtremor observations in this region were made on July 12, 13 and 15, 1982, with circular arrays 1, 2, and 3, as shown in Fig. 1. These three arrays fall almost along a line oriented in an east-west direction. Each array consists of 9 vertical component velocity sensors in three concentric circles with radii of about 87, 116 and 231 m, separately. The sensor spacings are about 100 to 400 m. The sensor's natural frequency is 1 Hz, and the damping factor is 0.67.

All measurements were conducted during the middle of the night (0 a.m. to 4 a.m.) in order to avoid the effects of culture noise as much as possible. The output of each sensor was amplified 100 to 1000 times. The signal was digital recorded at a rate of 200 samples/sec, and then converted to 12 bits binary and 4 bits gain ranging and stored on magnetic cassette tapes.

3. METHOD OF ANALYSIS

A seismic array is a set of seismographs distributed over an area of the

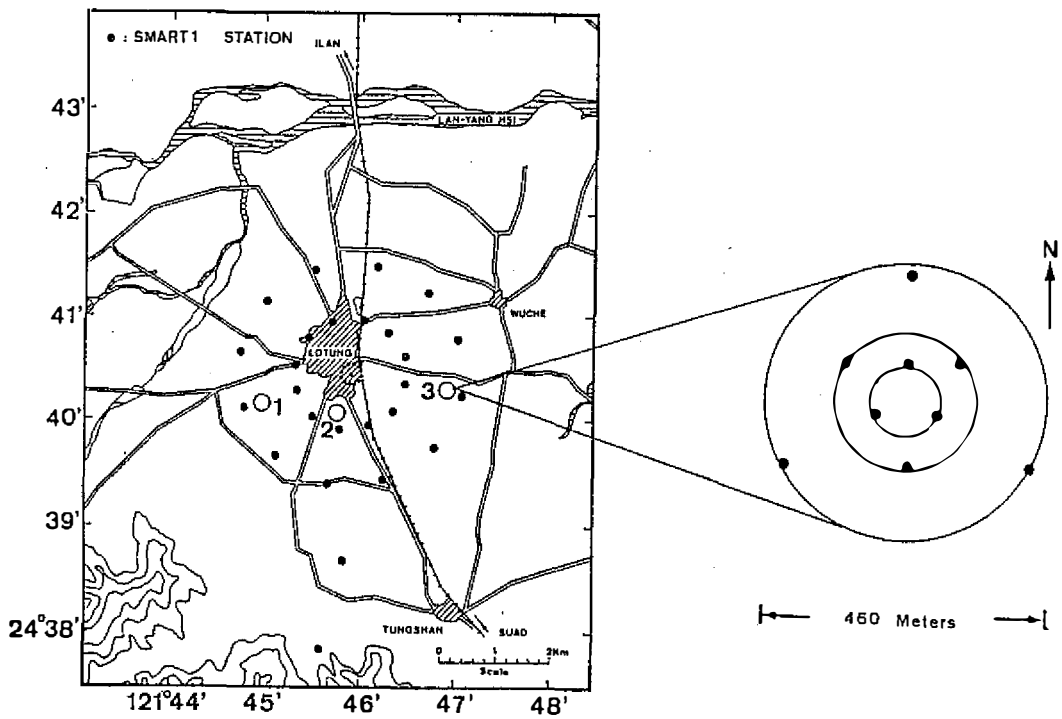

Fig. 1. The SMART1 array and small array configuration ('O' denotes the observation sites of the microtremor).

Earth's surface with a spacing narrow enough, that the signal waveform may be correlated between adjacent seismographs. It is useful for studying detailed characteristics of wave field propagation across the array (Aki and Richards, 1980). The f-k power spectrum is a function of frequency and wavenumber. It will tell us the directions of approach to the array and velocities of the waves propagated across the array.

To estimate the f-k power spectra, two methods were developed. One is the Beam-Forming Method (BFM) (Lacoss *et al*, 1969) and the other is the Maximum-Likelihood Method (MLM) (Capon, 1969). Fig. 2a is an example of a BFM array response for array 2. It can be seen that the BFM in the wavenumber space strongly depends on sensor location and it also has a prominent sidelobe. In the presence of multipath propagation, the large sidelobe effects can't be clearly recognized. Fig. 2b is an example of an MLM array response for array 2. It shows a more rapid collapse around the power peak and suppresses the sidelobes caused by finite array configuration. The resolution of MLM depends not only on sensor location but also on signal-to-noise ratio (SNR). As incoherence noise increase with no improvement of resolution by the MLM can be achieved. Mack and Filnn (1971) suggested two mechanisms which cause coherence loss–independent additive noise and propagation

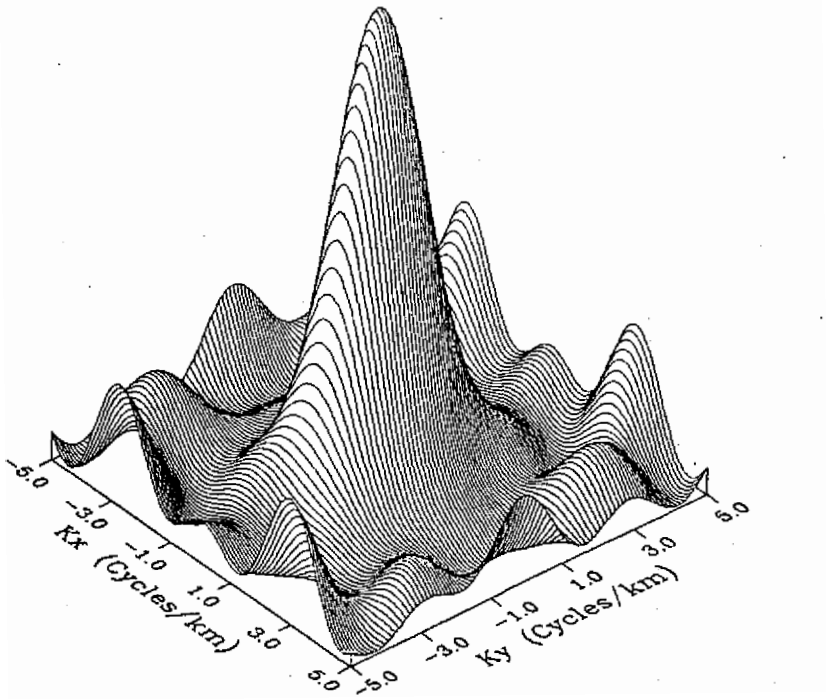

Fig. 2. (a) The BFM array response for array 2.

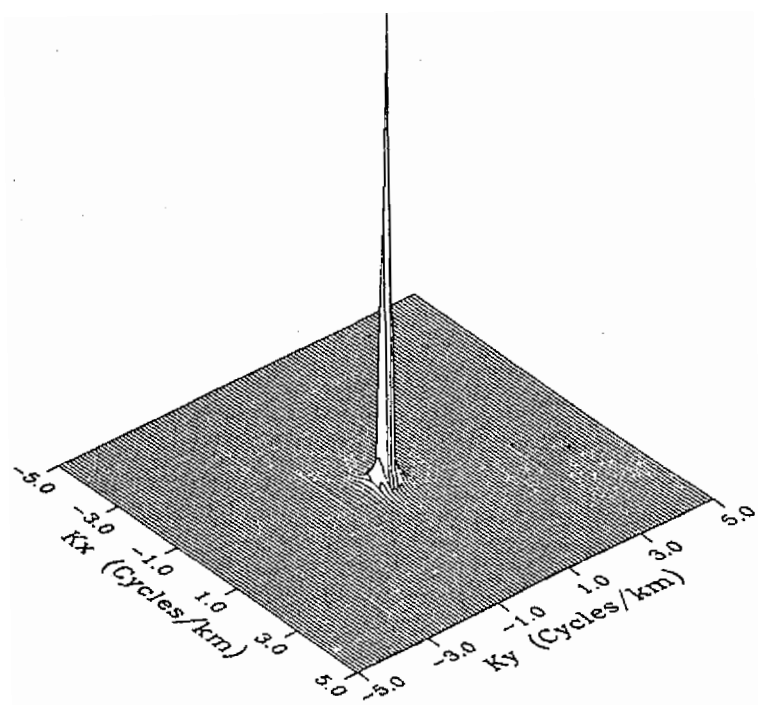

Fig. 2. (b) The MLM array response for array 2.

effects. Wood and Lintz (1973) discussed the resolving power of an array and concluded that it clearly depends on three factors: the diameter of an array, the spatial distribution of the sensors, and the correlation between the two events to be resolved. It appears that the MLM is the better method for processing two dimensional array data for high resolutions in the presence of multipath interference. Therefore, it is most suitable for background noise studies.

The power spectrum at frequency f and vector wavenumber k for an array of N sensors by MLM is given by

$$P(f,k) = [\sum_{i,j=1}^{N} \phi_{ij}^{-1}(f) exp(i\vec{k} \cdot \vec{r}_{ij})]^{-1} , \quad (1)$$

where

N = number of sensors.

$\phi_{ij}(f)$ = cross-power spectrum between ith and jth sensors at frequency f.

$\vec{r}_{ij} = \vec{r}_j - \vec{r}_i$ where $\vec{r}_i$ and $\vec{r}_j$ are the position vectors of the ith and jth sensors.

$\phi_{ij}^{-1}(f)$ = is the element of the corresponding inverse for the matrix $\phi_{ij}(f)$.

4. DATA PROCESSING

For some reason, the 9 sensors of each array did not always work. The number of effective sensors that corresponds with each observation is shown in Table 1. In order to avoid spurious results in the wavenumber domain caused by spatial aliasing, the wavelength we analyze must be greater than twice the minimum sensor spacing, i.e. 200 m.

The computation of f-k power spectrum was done using the following steps:

(1) To compute the cross-power spectra. The method discussed by Capon (1969) was used. For resolution and stability of the estimated power spectrum, we selected 100 seconds' data length for arrays 1 and 2, then divided these time series into 8 segments, each segment being 12.5 seconds; for array 3, we selected 300 seconds' data length and divided the time series into 32 segments, each time segment being 12.5 seconds. The data length and segment which we divided is shown in Table 1. In each time segment Hanning's window was used before transforming each segment into the frequency domain. Cross-power spectrum estimates were obtained by multiplying in the frequency domain and then averaging the results.

(2) The MLM is based on the inverse of the coherency matrix $\phi_{ij}(f)$ in Eq. (1). An additional condition for the successful application of the MLM method is that the coherency matrix be nonsingular. Capon (1969)

Table 1. The observation time and data selection conditions for each array.

Array No.	OT	N	M	DL	R
1	07 12 2:10	5	8	12.5	0.00
1	07 12 2:30	8	8	12.5	0.01
2	07 13 1:40	9	8	12.5	0.01
2	07 13 2:00	6	8	12.5	0.00
2	07 13 3:50	9	8	12.5	0.01
2	07 13 4:00	6	8	12.5	0.00
2	07 13 4:05	9	8	12.5	0.01
3	07 15 0:45	6	32	12.5	0.00

OT : Observation time.
N : Number of stations used at each observation time.
M : Number of time segments to be divided.
DL : Data length of each time segment (in seconds).
R : The small amount added to the diagonal term, when **M<N.**

showed that a necessary condition for nonsingularity is that the number of blocks (M) used in estimate $\phi_{ij}(f)$ must be greater than or equal to the number of sensors (N). A nonsingular matrix is assured if a small amount of incoherent noise is added to the diagonal element $\phi_{ij}(f)$. In order not to influence the resolution on of wavenumber, this small amount (R) added was 0.01, when $M < N$, as shown in Table 1.

(3) The f-k power spectrum is displaced here as $-10 \times Log_{10}(P/P_{max})$ contours in the wavenumber domain $|k| \leq 5$ cycles km^{-1}, where P/P_{max} is the ratio of f-k power at each coordinate (k_x, k_y) to peak power. The wavenumber space consists of 51 × 51 grids; contouring from 0 to 14 *db*, with an interval of 2 *db*. In the diagram, the '•' mark indicates the peak power. The velocity V was estimated by

$$V = f/\sqrt{k_{x_0}^2 + k_{y_0}^2}, \tag{2}$$

where k_{x_0} and k_{y_0} are corresponding to peak power positions in the wavenumber space.

5. RESULTS

Figs. 3 and 4 are some examples of f-k power spectra at arrays 1 and 2, respectively. Fig. 3 shows the f-k power spectra at frequencies 0.64 to 1.52 *Hz* for the microtremors observed by array 1. The maximum peak is found to

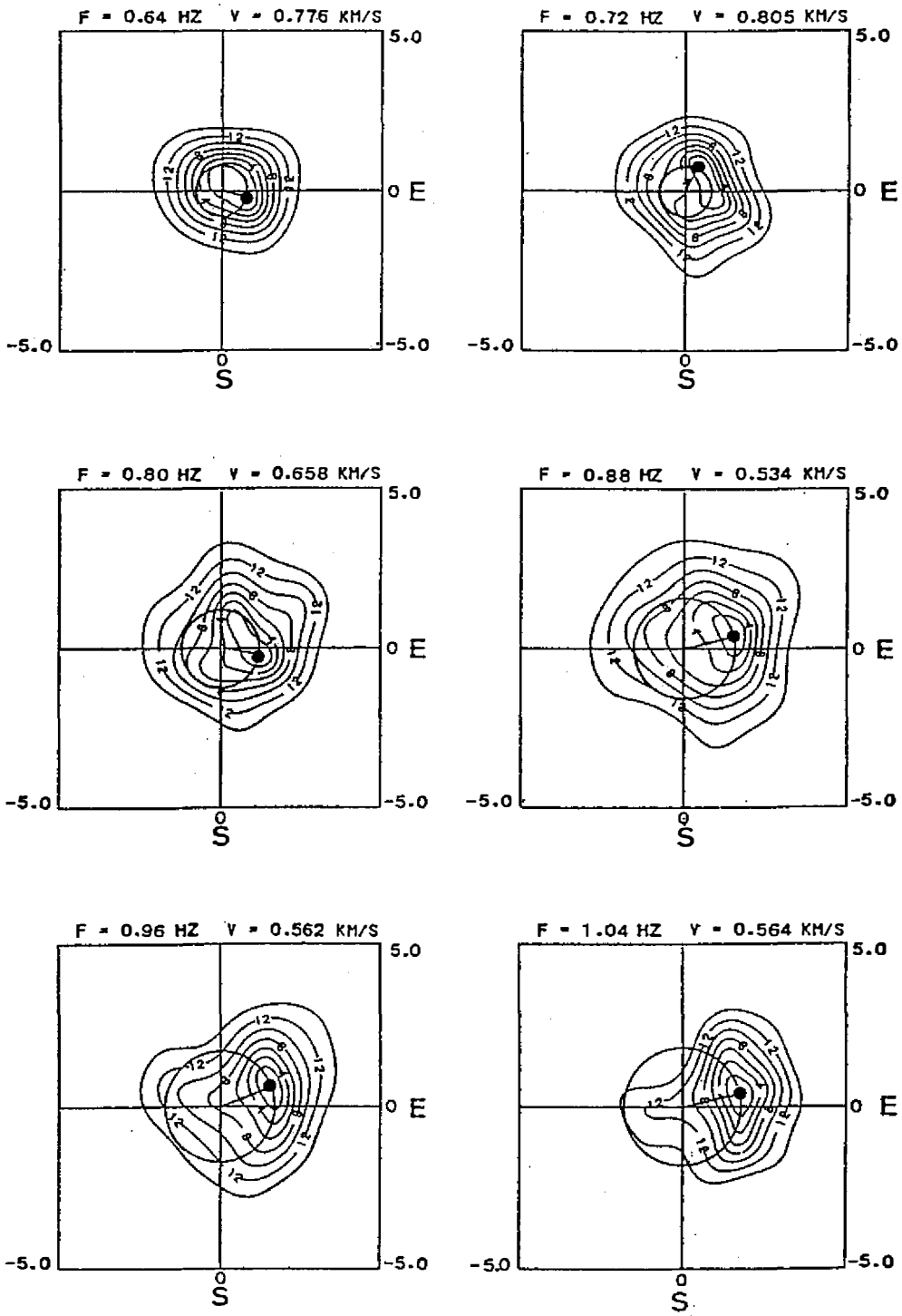

Fig. 3. (a) The f-k power spectra by MLM at frequencies 0.64 to 1.04 Hz for array 1. Solid dots denote locations of the highest peaks.

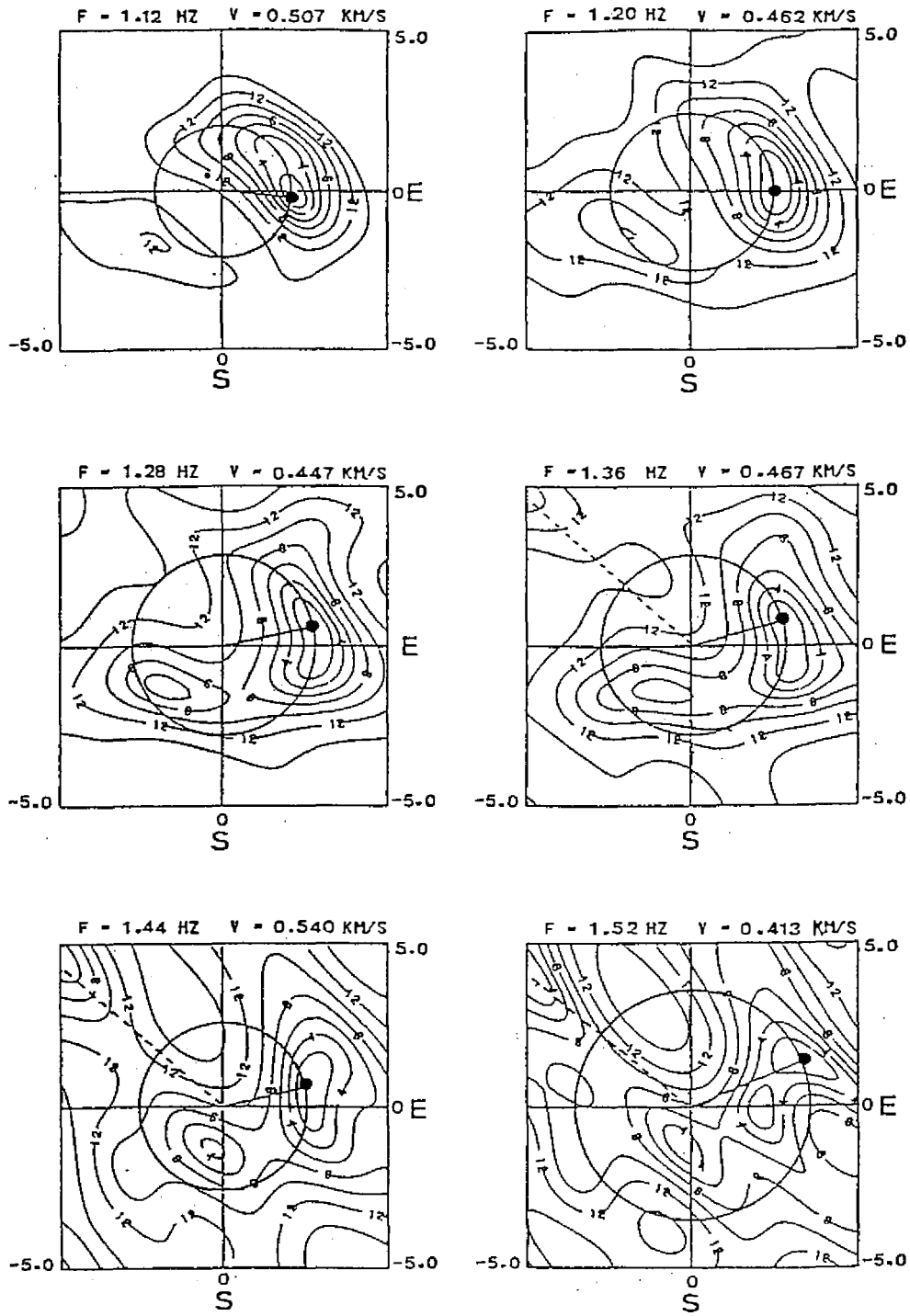

Fig. 3. (b) The f-k power spectra by MLM at frequencies 1.12 to 1.52 Hz for array 1. Symbols denote the same as in *Fig.* 3a.

be located in almost the same position (in the first quadrant) with a similar spectrum shape at all frequencies, especially at 0.8 to 0.96 Hz and 1.28 to 1.52 Hz. It probably suggests that the microtremors are produced by the same source. The second peak appears in the third quadrant at frequencies of 1.04 to 1.52 Hz with higher apparent velocities than that of the maximum peak. When examined, there was a microearthquake that occurred during that time. The epicenter was located 24°2′ N and 121°11′ E. We suggest that the peaks in the third quadrant were associated with this microearthquake. It is obvious that the f-k technique could distinguish the mixture of both surface and body waves, if they existed. At frequencies of 1.44 to 1.52 Hz, there existed weak signals in the second quadrant (dashed line). It can be justified that they were caused by the sidelobes of the array response.

Fig. 4 shows the f-k power spectrum of the microtremors detected by array 2 at frequencies 0.88 to 1.76 Hz. They can be divided into three groups. The first is 0.88 to 1.28 Hz; the second is 1.36 to 1.44 Hz; and the third is 1.52 to 1.76 Hz. The f-k power spectra of the second and third groups are more complicated than those of the first and second groups. The direction of the maximum peak changed back and forth from the first quadrant to the fourth quadrant. We suggest that the change of azimuth was due to energy being scattered from the propagation path. This scattering may have been associated with local structure irregularities. It can be seen that another peak is located at the k-axis for frequencies 1.52 to 1.76 Hz. Comparing the second peak to the maximum peak at each frequency, we can see that they have a different direction of approach, but have nearly the same velocity.

At array 3, the maximum peak of the f-k power spectra was always at the fourth quadrant (not shown here). It probably suggests that as the microtremors in this area are very stable, they must be produced by the same source.

From the above analysis, we see that all of the maximum peaks of the f-k power spectra are located at the first or fourth quadrant. This means that the energy of the microtremors approaches from the northeast or southeast direction. The spectrum shape changes with frequency gradually. At frequencies of less than 1.04 Hz, there exists a coherence energy across the array, and at frequencies greater than 1.04 Hz, the energy of microtremors may be scattered by local structure irregularities, and the coherence decreases owing to the sensor spacing used.

6. DISCUSSION

As mentioned before, the f-k power spectra indicate that the microtremors are propagated into the small arrays from northeast or southeast directions.

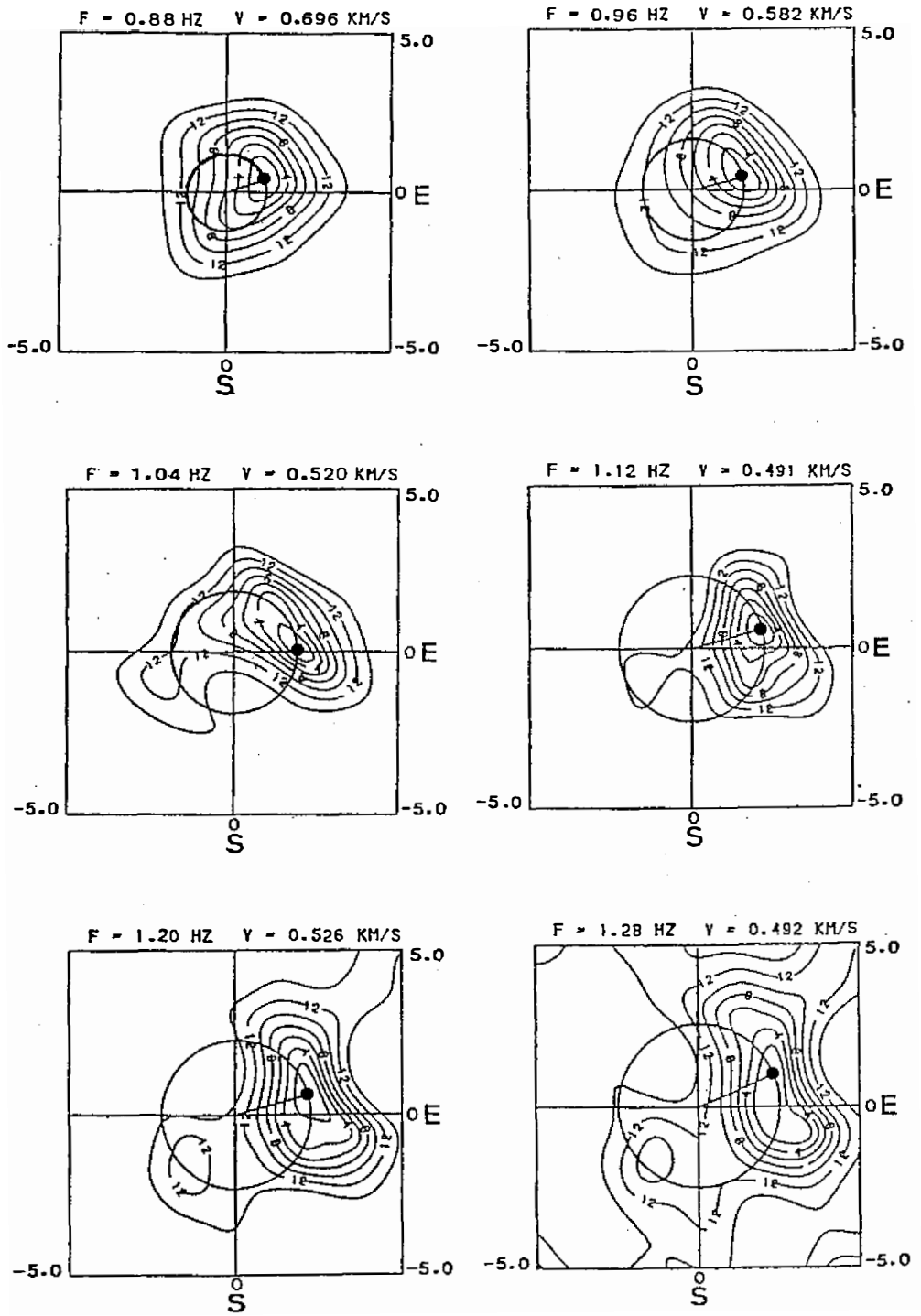

Fig. 4. (a) The f-k power spectra by MLM at frequencies of 0.88 to 1.28 Hz for array 2. Symbols denote the same as in *Fig.* 3a.

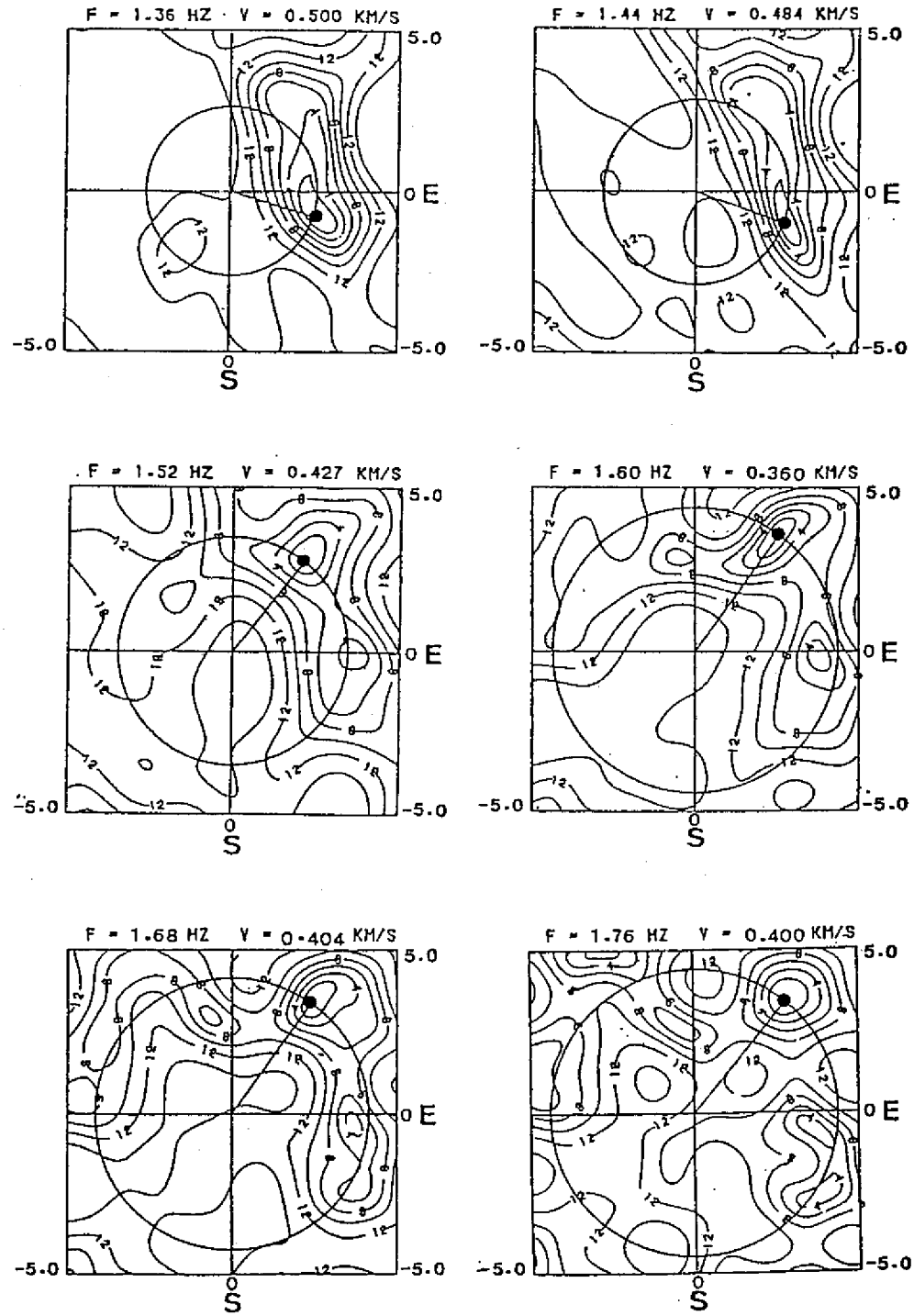

Fig. 4. (b) The f-k power spectra by MLM at frequencies of 1.36 to 1.76 Hz for array 2. Symbols denote the same as in *Fig.* 3a.

There are many possible origins we must take into consideration such as traffic (vehicles, trains), and coastal effects or streams near the observation sites. In the following paragraphs, we will discuss these possible microtremor origins in detail.

(1) During the observation period (middle of the night), the traffic of the array region is limited. Lee (1973) studied the seismic noise caused by traffic, and showed that its frequency is always greater than 0.5 Hz. Morever, when the sensor is located 30 to 40 m away from the highway, only weak noise can be observed. It attenuates rapidly with distance. In our experiment, the distance between the highway and the sensors is at least 170 m; therefore, traffic noise is too weak to be detected. Besides, the noise must be of very short duration of time compared to our observation time. The process of carefully selecting data segments (100 seconds) to compute f-k power spectra will also avoid the contamination.

(2) The nearest distance of array 1, 2 and 3 is about 630, 2600 and 3000 m from the Lanyang river, respectively. Iyer and Hitchcock (1976) reported that a flowing river generates noise at frequencies above 6 Hz, and attenuates by about 12 db at 1000 m from the river. From our f-k estimate, it is obvious that no coherence energy above 6 Hz could be seen.

(3) Average phase velocities of array 1, 2 and 3 at frequencies 0.8 to 1.76 Hz, 0.72 to 1.84 Hz and 0.72 to 1.52 Hz are 857 to 360 $m\ s^{-1}$, 788 to 375 $m\ s^{-1}$ and 699 to 316 $m\ s^{-1}$, respectively (Table 2; Fig. 5). In order to identify the wave types of the microtremors within the above frequency bands, the seismic velocity structure beneath the array area must be known. P-wave velocity structures beneath the Lanyang plain and the SMART1 have been studied by Chiang (1976) and by Wen and Yeh (1984), respectively. The subsurface structure of the SMART1 area from the top can be summarized as follows: (a) The soil layer has P-wave velocity of about 430 to 760 $m\ s^{-1}$ with a thickness of about 3 to 18 m; (b) The alluvium layer has a P-wave velocity of about 1400 to 1700 $m\ s^{-1}$ with a thickness of about 30 to 60 m; (c) The third layer has a P-wave velocity of about 1800 to 2000 $m\ s^{-1}$ with a thickness of about 170 to 540 m; (d) The Miocene basement has a P-wave velocity of about 3300 to 4000 $m\ s^{-1}$. If we suggest that $V_s = \sqrt{3}V_p$, the S-wave velocity of the basement is calculated at about 2000 $m\ s^{-1}$. The phase velocities obtained for microtremors are less than the S-wave velocity of the basement at any SMART1 region (Table 2) and are of normal dispersion (Fig. 5). This may suggest that the microtremors are Rayleigh waves.

According to the above considerations, we exclude the origins caused by

traffic and stream, and suggest that the origin of microtremors at the SMART1 area may be caused by the effects of the Pacific ocean on the coast. The first column of Table 2 shows the average phase velocities of each array obtained from f-k estimate. Compare the results of array 1 and 2. It can be seen that the phase velocity corresponds with each frequency and is nearly the same. At frequencies between 0.96 to 1.04 Hz, both arrays have a velocity drop from 703 to 585 $m\ s^{-1}$ and 689 to 558 $m\ s^{-1}$, respectively. For array 3, there also exists a velocity anomaly from 669 to 468 $m\ s^{-1}$ between frequencies 0.72 to 0.8 Hz; and at frequency 0.8 Hz the velocity is 468 $m\ s^{-1}$, which is much less than that of array 1 and 2, at the same frequency.

Table 2. The phase velocity and effected depth corresponding with each frequency for the three arrays.

Array No.	1		2		3	
Frequency (Hz)	velocity (m/s)	depth (m)	velocity (m/s)	depth (m)	velocity (m/s)	depth (m)
0.72	----	----	717	332	699	309
0.80	857	357	788	328	468	195
0.88	788	298	700	265	376	142
0.96	703	244	689	239	410	142
1.04	585	188	558	179	373	120
1.12	532	158	512	152	328	98
1.20	525	146	497	138	333	92
1.28	426	111	497	129	316	82
1.36	444	109	476	117	336	82
1.44	462	107	481	111	340	79
1.52	404	89	463	101	359	79
1.60	370	77	405	84	----	----
1.68	374	74	412	82	----	----
1.76	360	70	377	71	----	----
1.84	----	----	375	----	----	----

If we suggest that the depth of a Rayleigh wave can be about one-third of its wavelength, the second column of Table 2 shows that depth corresponds with each frequency at each array. Their range is between 357 and 70 m. From Wen and Yeh (1984), the average thickness from surface to bedrock is about 410 m, for the SMART1 area which is larger than the greatest depth Rayleigh waves can penetrate. Therefore, the propagation path of a Rayleigh wave caused by microtremors is mainly controlled by the alluvium layer and Pleistocene formation, for the SMART1 area.

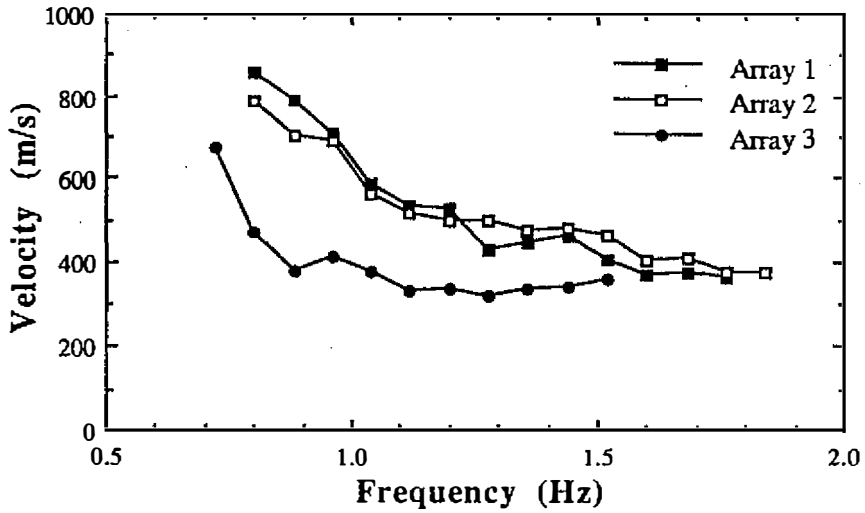

Fig. 5. The average phase velocities of microtremors obtained by MLM f-k spectra at arrays 1, 2 and 3.

The average P-wave velocity of the Pleistocene formation is 1900 $m\ s^{-1}$ and we suggest the Rayleigh wave velocity is 0.92 times of that S-wave. According to velocity anomalies, we may divide the subsurface structure into two layers (Table 3):

Table 3. The geological conditions of three arrays obtained form f-k estimates.

Array No.	Layer 1			Layer 2		
	Thickness (m)	S-velocity (m/s)	Poisson ratio	Thickness (m)	S-velocity (m/s)	Poisson ratio
1	113	488	0.465	187	851	0.375
2	112	499	0.462	179	787	0.395
3	110	396	0.477	198	686	0.425

(1) First layer (from the top): From array 1 to array 3, the thicknesses are 113, 112 and 110 m; the S-wave velocities are 488, 499 and 396 $m\ s^{-1}$; the Poisson ratios are 0.465, 0.462 and 0.477, respectively.

(2) Second layer (below the first layer): From array 1 to array 3, the thicknesses are 187, 179 and 198 m; the S-wave velocities are 851, 787 and 686 $m\ s^{-1}$; the Poisson ratios are 0.375, 0.396 and 0.425, respectively.

It is obvious that the S-wave velocities of array 3 have significant differences among these arrays. It may be due to the differences of the rock's physical

properties beneath array 3. Our results didn't show the geological boundaries like Wen and Yeh (1984). If we increase the array's dimension and decrease the distance between adjacent sensors in this study, we may realize the longer and shorter wavelengths of microseisms, and could obtaine more detailed geological conditions for the SMART1 area.

7. CONCLUSIONS

Three separate small circular arrays were installed in the vicinity of the SMART1 area, on July 12, 13 and 15, 1982, to record the microtremors at the site of the SMART1 in northeastern Taiwan. In this study frequency-wavenumber analysis was used to investigate the noise field. The analysis covered the frequency range from 0.72 to 1.84 Hz. The origin and characteristics of microtremors can be summarized as below:

(1) At a frequency range between 0.8 to 1.76 Hz, 0.72 to 1.84 Hz and 0.72 to 1.52 Hz, for array 1, 2 and 3, respectively, there always exists a coherence energy across the array in north-east /or south-east directions. We suggest that they may be generated by the effect of the Pacific Ocean on the coast.

(2) At frequencies 0.72 to 1.84 Hz, the phase velocities obtained from f-k estimates are less than the S-wave velocity of the basement (Lushan Formation), and are at normal dispersion, thus we could identify the waves types as Rayleigh waves. At frequencies less than 0.64 Hz (not shown here), the wavelength of the microtremors are about four or five times the array diameter, therefore the array would not be able to give adequate wavenumber resolution. At frequencies greater than 1.84 Hz, no organization of the microtremors could be detected at the sensor spacing used.

(3) According to velocity anormalies and dispersion curves (Fig. 5), the subsurface structure of the SMART1 area could be divided into two layers (Table 3): (a) First layer (from the top): the thicknesses are 113, 112 and 110 m; the S-wave velocities are 488, 499 and 396 $m\ s^{-1}$; the Poisson ratios are 0.465, 0.462 and 0.477; (b) Second layer (below the first layer): the thicknesses are 187, 179 and 199 m; the S-wave velocities are 851, 787 and 686 $m\ s^{-1}$; the Poisson ratios are 0.375, 0.396 and 0.425. It can be seen that the structure beneath these arrays is nearly flat, but the S-wave velocities beneath array 3 are less than those beneath arrays 1 and 2. This may be due to the different physical properties of the geological formations.

Acknowledgements. The authors would like to express their sincere thanks

to Mr. K. L. Wen and Miss M. R. Sun for their help with computer program use and with data collection. This research was supported by the National Science Council of the Republic of China.

REFERENCES

Aki, K. and P. G. Richards, 1980: Quantitative Seismology Theory and Methods, W. H. Freeman and Co., San Francisco.

Asten, M. W. and J. D. Henstridge, 1984: Array estimates and the use of microseisms for reconnaissance of sedimentary basin. *Geophysics*, **49**, 1828-1837.

Bungum, H., R. Eivind and B. Leif, 1971: Short-period seismic noise structure at the Norweigian array. *Bull. Seismol. Soc. Am.*, **61**, 357-373.

Capon, J., 1969a: Investigation of long-period noise at the large aperture seismic array. *J. Geophys. Res.*, **74**, 3182-3194.

Capon, J., 1969: High-resolution frequency-wavenumber spectrum analysis. Proc. IEEE., 57, 1408-1418.

Chiang, S. C., 1976: A seismic refraction prospecting of the Ilan Plain (in Chinese). *Mining Tech.*, **14**, 215-221.

Douze, E. J. and S. J. Laster, 1979: Seismic array noise structure at the Roosevelt Springs, Utah, geothermal area. *Geophysics*, **44**, 1570-1583.

Haubrich, R. A. and McCamy, 1969: Microseisms: coastal and pelagic sources, *Rev. of Geophys.*, **7**, 539-571.

Horike, M., 1985: Inversion of phase velocity of long-period microtremors to the S-wave-velocity structure down to the basement in urbanized area. *J. Phys. Earth*, **39**, 59-96.

Iyer, H. M. and T. Hitchcook, 1974: Seismic noises measurement in Yellowstone National Park. *Geophysics*, **39**, 389-400.

Kanai, K. and T. Tanaka, 1961: On microtremors. *Bull. Earthq. Res. Inst.*, **39**, 97-114.

Katz, L. J., 1976: Microtremors analysis of local geological condition. *Bull. Seismol. Soc. Am.*, **66**, 45-60.

Lacoss, R. T., E. J. Kelly and M. N. Toksöz, 1969: Estimation of seismic noise structure using array. *Geophysics*, **29**, 21-38.

Lee, T. Q., 1974: The studies of background seismic noise due to traffic (in Chinese). M. S. Thesis, National Central Unvi., R.O.C..

Liaw, L. J. and T. V. McEvilly, 1979: Microseisms in geothermal exploration studies in Grassy Valley, Navada. *Geophysics*, **44**, 1097-1115.

Mack, R. and E. A. Filnn, 1971: Analysis of the spatial coherence of short-period acoustic-gravity waves in the atmosphere. *Geophys. J. R. astr. Soc.*, **26**, 255-269.

Oppenheimer, D. H. and H. M. Iyer, 1980: Frequency-wavenumber analysis of geothermal microseisms at Norris Geyser baisn, Yellowstone National Park, Wyoming. *Geophisics*, **45**, 952-963.

Woods, J. W. and P. R. Lintz, 1971: Plane waves at small array. *Geophysics*, **38**, 1023-1041.

Wen, K. L. and Y. T. Yeh, 1984: Subsurface structure under the SMART1 array. *Bull. Inst. Earth Sic., Academia Sinica*, **4**, 51-72.

羅東強震儀陣列區微地動的特性

黃文紀　葉永田
中央研究院地球科學研究所

摘　要

1982年7月12，13和15日，我們在羅東強震儀陣列區(簡稱SMART1)，利用三個位置不同的小型陣列，從事了數次的微地動測記，以期對該地區的地動雜訊有所了解。本文是利用頻率一波數(Frequency-Wavenumber)的分析方法，研究微地動的來源與特性。分析結果顯示：在頻帶0.6赫至1.84赫之間，微地動的來源可能由東側太平洋海岸浪潮所造成，且微地動的特性是表面波。由微地動的速度頻散曲線我們也大略推測陣列區的地下構造。由地表至深度300公尺左右，大致可分成二個層次，第一層的厚度約爲110公尺，其S波的速度約爲是380公尺／秒至500公尺／秒。第二層的厚度約爲200公尺其S波的速度爲700公尺／秒至850公尺／秒。